Article

Characterization and Distribution of Pyrogenic Carbon in a Fraction of Archaeological Black Earth from Caxiuanã

Milena Carvalho Moraes,[*,a] *Vanda Porpino Lemos,[a] Dorsan Santos Moraes[b] and Cláudio Nery Lamarão[b]*

[a]*Instituto de Ciências Exatas e Naturais and* [b]*Instituto de Geociências, Universidade Federal do Pará, Campus Guamá, 66075-110 Belém-PA, Brazil*

This study aims to determine the atomic ratio of O/C in an archaeological black earth (ABE) profile of the Ilha de Terra site, a region of Caxiuanã in the Pará State, Brazil, to determine the types of pyrogenic carbon (PyC) particles and to infer the source of biomass and burning temperature necessary to produce the PyC. The O/C ratios were monitored using scanning electron microscopy combined with energy dispersive spectroscopy (SEM/EDS). The results indicated atomic ratios for clay, silt and fine sand fractions that were between those registered for the PyC particles types: condensed combustion (CC) (0.09, 0.1, 0.13), charcoal (0.32, 0.31, 0.34) and char (0.43, 0.45, 0.52). CC is the predominant type of particle found because of the high firing temperature (> 350 °C), which is consistent with the probable biomass sources of wood, cellulose and lignin.

Keywords: pyrogenic carbon, black earth, O/C atomic ratio, condensed combustion

Introduction

Pyrogenic carbon (PyC) is the term widely used for highly condensed carbonaceous material originating from the incomplete combustion of fossil fuels and biomass,[1,2] and it includes a wide variety of fire-derived polymeric, aromatic and graphitic carbon forms, such as char, charcoal, soot and graphite.[3] Other terms used to describe PyC are black carbon, elemental carbon or carbon plant.[4] PyC is an important component of natural organic matter,[5,6] which is intimately tied to carbon and global oxygen cycles,[7] and may play a significant role in global climate change[8] because it is highly resistance to a range of chemical oxidants.[6]

The pyrogenic carbon particles are also defined as materials that vary in the composition of partially carbonized plant materials that still retain the physical structure of coal, soot and graphite. Generally, there is not a dividing point between the different physical and chemical properties of the PyC or a boundary between different combustion by products. Thus, each material has a different definition based on different areas of studies and technical recognition.[9]

PyC is a highly recalcitrant form of organic carbon that is resistant to decomposition[10,11] and is characterized by clusters of aromatic rings, but it varies in size and in the presence of other elements (N, O) and functional groups.[12]

The main difficulty in the identification and quantification of PyC is the heterogeneity of the source material, which is related to the degree of fire exposure and the mechanism of production.[13-15] Based on these characteristics, the chemical composition of PyC is represented by a range of atomic ratios of carbon to other elements, such as oxygen, hydrogen, nitrogen, chlorine and sulfur.[15]

The occurrence of PyC as a carbonaceous material with continuous chemical variations is the target of studies by many research groups. PyC particles were recognized in reference materials, such as in aerosols from the atmosphere,[16] in soils,[17,18] in terrestrial sediments,[19] in biomass,[20] and in archaeological black earth.[10,11,21,22]

Archaeological black earth (ABE) soils are formed from intense human activities, such as the burning of biomass and nutrient deposition in indigenous settlements in the Amazon, resulting in changes in the chemical and physicochemical properties of the original soil.[23-25] ABE have been discovered in many parts of the world, and are usually observed near rivers and highlands as spots that are darker than adjacent soils.[26] The main ABE are located in the Brazilian Amazon and are also found in Bolivia, Ecuador, Colombia, Guyana, Peru and Venezuela.[27,28]

These soils show elevated concentrations of Ca and P that are associated with deposits of organic material of

*e-mail: mina.carvalho@gmail.com

animal origin, such as Cu, Zn, Mn and Fe in areas where plant residues have been deposited. The soils have also been reserved for ceremonies or for the production of artifacts,[29,30] ceramic fragments[31,32] and black carbon[6,10,11] (also referred as pyrogenic carbon)[5,13,17] that is a natural component of organic matter. When exposed to high temperatures, the neoformation of polyaromatic compounds is induced, increasing the stability of humus[6,10,11] and soil aggregation.[33]

In soils containing carbonaceous residues of different types and origins, such as ABE soil, the identification of PyC by reliable methods has became very important. Methods include the determination of the O/C atomic ratio, which is based on the combination of micromorphological and elemental analysis by scanning electron microscopy combined with energy dispersive spectroscopy (SEM/EDS),[17,34] and the determination of H/C and C/N via elemental analysis using the combustion method.[35] These methods should provide the contributions from PyC biomass sources and the chemical properties.[13] These atomic ratios may indicate the components from the chemical variation continuous spectrum defined for the pyrogenic carbon[9] and provide the temperatures at which the organic material of the ABEs were exposed to during PyC formation.[8,13]

The O/C ratio is suitable to differentiate between the PyC and soil organic matter,[11] and the ratio is a powerful tool for the PyC source assignment of soot and fly ash in environmental samples.[17,36]

The differences observed in the O/C atomic ratio of the same class of pyrogenic carbon can be a problem for the interpretation of their pattern of distribution and in the restoration of human behavior from an archaeological site.

The characteristics mentioned above regarding the O/C ratios are of great relevance to archaeological site studies, such as the Ilha de Terra site from the Caxiuanã Region Conservation Unit, in the Pará State, Brazil. The present study contributes to the PyC characterization and classification by determining the O/C atomic ratios using SEM/EDS for different samples fractions from the ABE profile. The ratios indicate the main morphological variability, the types of PyC particles and the typical ABE of the soils, and they also infer the biomass source and burning temperature that is likely to produce the pyrogenic carbon (PyC) and its distribution in the size fractions via the ABE profile.

Experimental

Location of the study area

The materials for this study were collected in the region of Caxiuanã, located in Pará, on the west side of Caxiuanã

Bay and downstream of the river Anapu and of the Xingu river bank, which includes the cities of Portel and Melgaço in the lower Amazon (Figure 1a). In the Caxiuanã Region, approximately 30 archaeological sites located on the banks of rivers and streams have been reported, and most are west of Caxiuanã Bay (Figure 1b). Local pre-colonial human occupation occurred in the higher areas of the landscape in relics of the lateritic crusts, which probably met the group's protection strategies and provided power resources, water and raw material for the manufacture of ceramic and lithic artifacts. These locations are often reused by contemporary populations for housing or grazing.[37,38] The sampling was carried out at the Ilha de Terra site, which is situated on the banks of Camuim Hole in the municipality of Melgaço-Pará at geographical coordinates 1° 42' 30'' S and 51° 31' 45'' W (Figures 1b and 1c).[38-40]
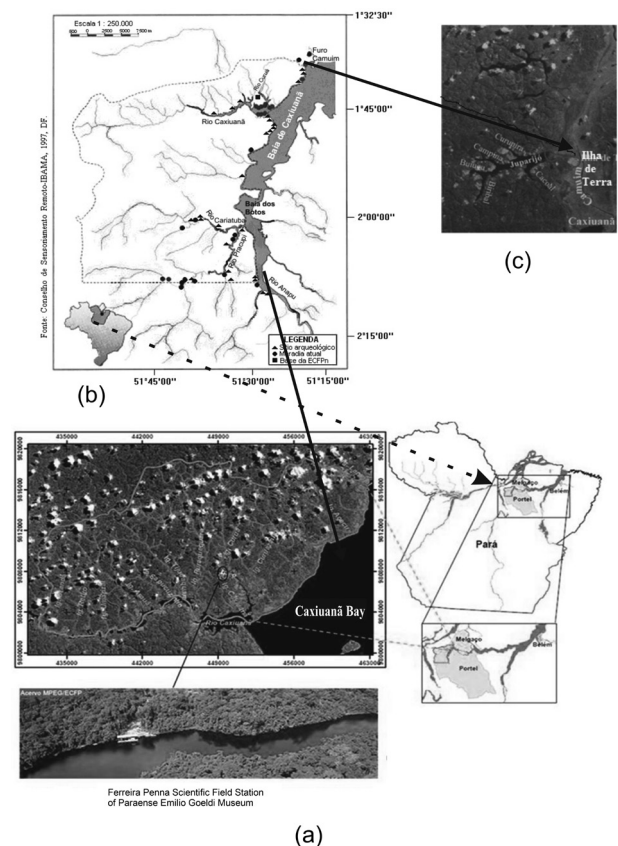

Figure 1. (a) Location of the Caxiuanã Region;[39] (b) archaeological sites and houses on the banks of the rivers and streams near Caxiuanã Bay;[40] (c) Ilha de Terra site on the banks of the Camuim Hole.[37]

Sample description from archaeological black earth profile

The archeological black earth (ABE) profile, which is 161 cm deep, is represented by A1 (0-7 cm), A2 (7-14 cm), A3 (14-29 cm), AB (29-57 cm), BA (57-89 cm) B1 (89-110 cm), B2 (110-135 cm) and B3 (135-161 cm)

Table 1. Characteristics of the ABE profile horizons and names of sub-samples of clay, silt, fine sand and coarse sand

Horizon	Thickness / cm	Color	Code color	Texture	Clay	Silt	Fine sand	Coarse sand
A1	7	black	10YR2/1	sandy	(A1)/1	(A1)/29	(A1)/15	(A1)/43
A2	7	black	10YR2/1	sandy	(A2)/2	(A2)/30	(A2)/16	(A2)/44
A3	15	dark brown	7,5YR3/2	sandy	(A3)/3	(A3)/31	(A3)/17	(A3)/45
AB	28	dark brown	7,5YR4/6	sandy	(AB)/4	(AB)/32	(AB)/18	(AB)/46
BA	32	brown	7,5YR4/3	sandy	(BA)/5	(BA)/33	(BA)/19	(BA)/47
B1	21	yellowish brown	10YR5/4	sandy-clay	(B1)/6	(B1)/34	(B1)/20	(B1)/48
B2	25	yellowish brown	10YR5/4	sandy-clay	(B2)/7	(B2)/35	(B2)/21	(B2)/49

horizons. The colors are characterized according to the Munsel codes,[41] and the textures are characterized by the changes in the levels of sand, silt and clay.[42] These features[43] and the designation given to the sub-samples of the soil fractions used in this study are listed in Table 1.

A black to brown color in the surface horizons is caused by the accumulation of organic matter in the ABE. In these horizons, the texture is sandy due to soil reworking by ancient inhabitants of the region.[43] In the deeper horizons, the color is yellowish brown, and the texture is sandy-clay due to the presence of goethite, hematite and clay minerals.[44]

SEM/EDS analysis for PyC characterization

Analysis using scanning electron microscopy combined with energy dispersive spectroscopy of X-ray (SEM/EDS) were applied for the PyC characterization in the ABE samples and were used based on prior studies that combined these methods for the PyC characterization in other types of soils.[17,34]

The steps involved in the PyC characterization are indicated in Table 2. The first step is the determination of differences in the carbonaceous particles using SEM to determine certain characteristics, such as geometric shapes, particle size and textural aspects of the fractionated and unfractionated samples, and to distinguish the PyC particles in the samples without previous treatment and after acid

treatment. These tests were performed only for samples without treatment to prevent the concentration of some elements on the PyC particles, as observed in the analysis of other soils.[17]

The second step included monitoring the O/C atomic ratio, as determined from a preliminary calculation of the oxygen bonded to carbon (O_C), without interference from the major and minor elements common in the Earth's crust, such as Na, Mg, Al, Si, K, Ca, Fe and P.

The O_C/C atomic ratio was calculated from equation:[34]

$$O_C = O[\%] - Na[\%] \times 0.5 + Mg[\%] \times 1 + Al[\%] \times 1.5 + Si[\%] \times 2 + K[\%] \times 0.5 + Ca[\%] \times 1 + Fe[\%] \times 1.176 + P[\%] \times 2.5 \qquad (1)$$

The O_C/C ratio was obtained by dividing the value of O_C by the concentration of C in each sub-sample. In the equation, different multiplying factors of element concentrations indicate their common valences within major crustal oxides. In the case of Fe, the factor is 1.176, indicating a common ratio of Fe^{II} (3.3%) and Fe^{III} (1.8%). In prior studies where PyC was found, this atomic ratio was expressed as O/C instead of the Oc/C.[17,34]

Conditions used in the analysis of SEM/EDS

Analysis by scanning electron microscopy (SEM) was performed on a LEO-1430 instrument. The samples were

Table 2. Steps involved in the PyC characterization and method evaluation used to obtain the O/C ratio

Step	Method	Reference	Step	Method	Reference
(1) Distinction of carbonaceous particles	scanning electron microscopy (SEM)	13,17,34,36	(4) rejection of O/C values	Dixon test	17,34
(2) Monitoring of O/C atomic ratio	energy dispersive spectroscopy (EDS)	17,34	(5) classification of PyC particles	values of O/C: > 0 and < 0.6	17,34
(3) Correction of matrix effects	position of the electron beam	17,34	(6) evaluation of precision and accuracy	based on standard deviation (SD) and relative error values	45

metallized with platinum on an aluminum support with a coating time of 2.0 min. In this case, an aluminum support was selected once contain negligible amounts of carbon and oxygen. The conditions for the analyses were: electron beam current: 90 μA, constant acceleration voltage: 20 kV, working distance: 15 mm. The semi-quantitative analyses of C, O, Ca, Mg, K, P, Si, Al, Fe and Na were performed using EDS with a Gresham detector and an analysis counting time of 30 s for the elements.

The conditions were the same for both samples and for the reference material for the EDS analysis during monitoring of the O/C ratios.

During the analysis, treatments were performed: the correction of matrix effects, which provide reference peaks of the elements. These corrections consider the analysis of the sample in a homogeneous polished session. In the analysis of pyrogenic carbon, this condition could not be met due to the variations in the shapes and dimensions of the particles. However, careful positioning of the electron beam on the particle may help and reduce the severity of the matrix effect on the analysis.[17] The application of the Dixon test or confidence test[34] both for the samples and for the reference material to reject the values of the O/C ratios that were considered dispersed in all the analysis results to eliminate outliers. After these steps, the PyC particles types were classified according to the O/C ratios reported for condensed combustion (CC), natural charcoal and char.[17,34]

Method precision and accuracy for obtaining the O/C ratio

The activated carbon Merck sample used as the reference has elongated particles that partially preserve its tubular shape (Figure 2), similar to those derived from
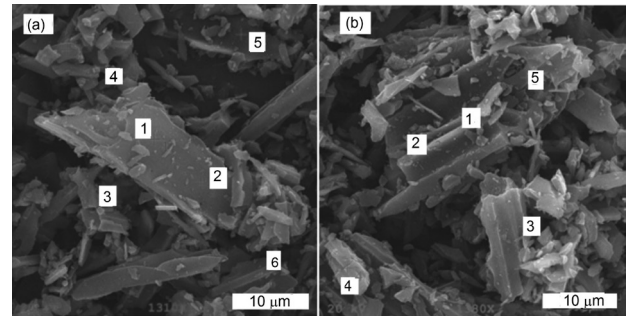

Figure 2. SEM micrographs of activated carbon samples obtained from secondary electrons.

plants observed in other samples containing PyC.[13,34] EDS analysis of the reference material indicated that the elements P, Ca and Fe were the main impurities. Based on the concentrations of C and O obtained in the analysis, the O/C was calculated from the equation. The calculation of the average values (m), standard deviation (SD) and variance (V) for the O/C ratios obtained from the PyC-characterized particles of activated carbon was used as the reference material for the archaeological black earth (ABE) samples. The accuracy and precision results were obtained via standard deviation and relative error, respectively.[45]

The O/C was determined from replicate analyses of reference samples using the same analytical conditions as for the ABE samples. Each replicate was taken at different points on the pyrogenic carbon fragments in the same sample holder. Therefore, the standard was an upper estimate of the variability, and it is likely that there was a real difference in the O/C between individual particles of pyrogenic carbon even within each sub-sample reference. This procedure was applied in another study of PyC.[17] In this study, the O/C values were between 0.023 and 0.086 and between 0.096

Table 3. Concentrations of the main chemical elements and O/C ratios in selected regions (a.1 to b.5) from samples of the reference material (activated carbon)

Element	a.1 / wt.%	a.2 / wt.%	a.3 / wt.%	a.6 / wt.%	b.1 / wt.%	b.2 / wt.%	b.3 / wt.%	b.4 / wt.%	b.5 / wt.%
C	88.64	88.67	87.46	87.81	88.56	93.02	88.13	92.2	86.4
O	10.07	10.05	11.5	11.01	10.42	6.04	10.96	5.98	12.88
Na	0.07	0.08	0.08	0.05	0.05	0.06	0.05	0.03	0.05
Mg	0.003	0.01	0.02	0.007	0.03	0.03	0.003	0.03	0.01
Al	0.038	0.007	0.01	0.06	not detected	not detected	0.011	0.09	0.001
Si	0.06	0.007	0.007	0.004	0.04	0.09	0.006	0.05	0.019
P	0.93	0.87	0.72	0.74	0.61	0.53	0.66	1.35	0.51
K	0.05	0.06	0.03	0.06	0.08	0.09	0.016	0.04	0.41
Ca	0.057	0.06	0.06	0.12	0.08	0.04	0.05	0.12	0.024
Fe	0.072	0.09	0.09	0.12	0.12	0.09	0.11	0.08	0.06
O/C	0.082	0.084	0.107	0.099	0.096	0.046	0.103	0.023	0.132

Table 4. Average values (m), standard deviation (SD), variance (V) and relative errors obtained for the O/C atomic ratios of the activated carbon Merck with comparison to other reference values

| Property	Reference material	Average value	n	Standard deviation	Variance	Relative error / %
O/C	activated carbon Merck	0.0586	4	0.03	0.0009	0.17
O/C	activated carbon Merck	0.1074	5	0.014	0.0002	0.024
O/C	commercial charcoal[17]	0.05	7	0.01	0,0001	–
O/C	coal from soft wood combustion[34]	0.11	8	0.02	0.0004	–

and 0.132 (Table 3). According to the PyC types, the first values were related to the condensates of combustion, and the second values were related to the charcoal.[17,34]

Average value, variance, standard deviation and relative error were calculated for the O/C data that corresponded to the two ratio ranges as mentioned above (Table 4). The SD and relative error values in this study suggested good precision and accuracy of the EDS analysis method used to obtain the O/C ratio.

Results and Discussion

Micromorphological and chemical data of the clay fraction

In the SEM, images from secondary electrons (Figure 3a) and backscattered electrons (Figure 3b) were observed for the sub-sample (A1)/1 that corresponded to the clay fraction of the A1 horizon. Other PyC characteristic features were also observed, such as oxidized material with some degraded cavities, which may have originated from plant waste burning or from the cellular structure of wood, according to the observations of other materials.[13]
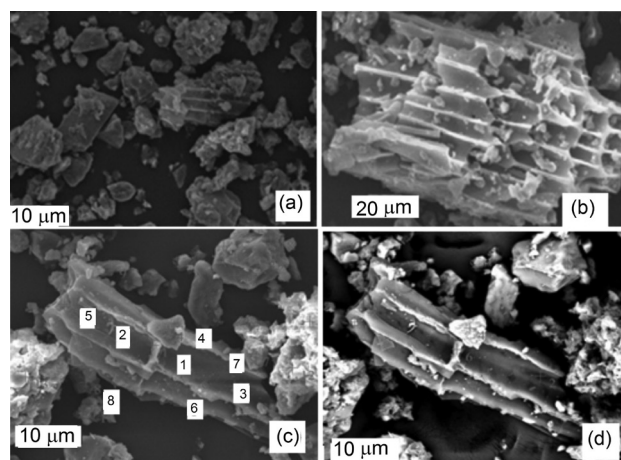
Figure 3. Images obtained from secondary electrons in the clay fraction from the A1 horizon in (a) and (c); from backscattered electrons in (b) and (d) showing the PyC particle residue from a burned plant.

The same features appear in another portion of the same sample and were observed in images obtained

from secondary (Figure 3c) and backscattered electrons (Figure 3d). In these images, it was possible to observe the difference between the efficiency and the use of signs by secondary electrons (SE) and backscattered (BSE) to study the PyC. A smooth surface was observed, classified as an elongated prism, where it is possible to observe the change in the hue of the particles by the darker spots that indicate the heterogeneity of the analyzed material.

For the particle shown in Figure 3c, large variations in the concentrations of the analyzed elements were found (Table 5). The concentrations of P, Ca, Mg, Na and K were higher than in various types of soils of the Amazon region but were similar to those obtained for ABE, and this is characteristic of the residues of bones and ceramic fragments.[31,32]

The chemical heterogeneity of the materials containing the particles of PyC was also observed in other studies.[21,34] In the sub-sample from the clay fraction of the A2 horizon (sample (A2)/2), the presence of circular particles and diatoms (image from secondary electrons) is observed (Figure 4a). These characteristics agree with studies that showed SEM images including the presence of circular structures with high levels of calcium and silicon, which were attributed to the remaining relics of diatoms or microorganisms.[21] PyC particles with circular morphologies observed in the (A2)/2 sub-sample may be due to a loss in volatile organic compounds in the firing processes and due to subsequent changes in the morphology of the reactive PyC particles. In this case, the particles can present forms of solid spheres or cenosphere fragments, depending on the time, temperature and other operating parameters of the combustion process. When the coal particles are organic components that are nonreactive with coal, the micrita fusinita do not soften the structure and spheroidal particles are not formed, they retain their original structure and morphology as the final particles obtain prismatic structures and elongated shapes, revealing characteristics of well-preserved wood fragments without structure.[13]

The same (A2)/2 sub-sample also shows PyC particles with porous channels, as show in Figures 4b and 4c (from backscattered electron). Some analyzed portions of these particles show that the concentrations of Si are higher than for the circular particles (Table 6).

Table 5. Concentration of the main chemical elements and the O/C ratio for selected regions of the (A1)/1 sub-sample clay fraction from the A1 horizon

Element	(A/1)1 / wt.%	(A/1)2 / wt.%	(A/1)3 / wt.%	(A/1)5 / wt.%	(A/1)6 / wt.%	(A/1)8 / wt.%
C	58.45	53.96	54.48	55.55	59.83	48.47
O	32.89	31.2	30.2	34.06	25.21	33.13
Na	0.06	0.08	0.2	0.06	0.17	0.1
Mg	0.56	0.66	0.78	0.42	0.66	0.2
Al	0.7	0.63	0.64	0.76	0.56	4.89
Si	1.24	2.34	1.41	3.79	1.41	7.38
P	0.61	1.22	1.1	0.91	1.02	0.99
K	0.083	0.16	1.15	0.1	0.07	0.26
Ca	5.07	9.42	10.69	3.95	10.8	1.31
Fe	0.33	0.32	0.35	0.36	0.26	3.26
O/C	0.37	0.22	0.21	0.32	0.12	0.06
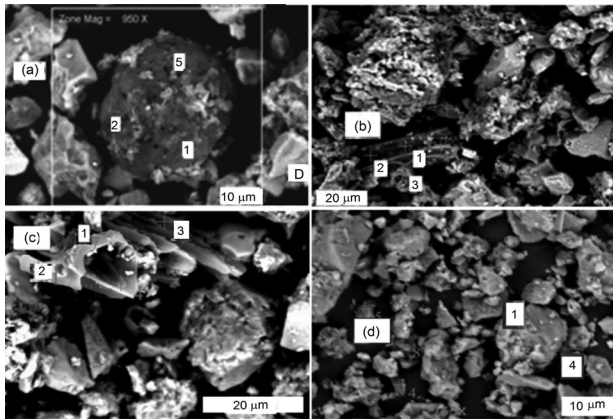
Figure 4. Micrographs showing PyC in the clay fraction from the A2 horizon: (a) circular particle and diatom/D; (b) and (c) tubular porous channels ((A2)/2 sample); and (d) particles having prismatic shapes ((A3)/3 sample).

For the A3 horizon, we observed changes in the shape of the PyC particles (Figure 4d) and a large increase in the Al content. For this horizon, the values obtained for the

O/C atomic ratios were rejected by the Dixon test. It was therefore not possible to characterize the PyC in the clay fraction of the ABE profile.

Micromorphological and chemical data of silt

The samples of the silt particles come in various forms, and we observed the presence of flat, sharp, prismatic and circular fragments, etc. (Figure 5).

In the analyzed sub-samples of the silt fraction in the A1 and A2 horizons, larger amounts of PyC particles (Figure 5) were observed than in the A3 and AB horizons. The EDS data (Table 7) show that point 4 of the 30/A2 sub-sample had the highest concentration of carbon of all the samples. The high concentrations of Si and Al in the samples of this fraction, as well as, in other analyzed samples, are likely due to waste minerals, such as kaolinite, which is common in various types of soil or plant debris. Other elemental concentrations were consistent with those expected from the ABE profile.

Table 6. Elemental analysis of the clay fraction from the A2, A3 and AB horizons

| Element	A2/2a1	A2/2a2	A2/2a5	A2/2b1	A2/2b2	A2/2c1	A2/2c2	A3/3-1	AB/4b5	AB/b6
C	59.5	63.3	59.6	52.07	51.55	57.18	46.76	48.65	43.1	46.4
O	34.53	31.3	35.4	38.27	36.03	34.47	35.44	35.5	17.9	28.1
Na	0.05	0.02	0.15	0.1	0.08	0.07	0.03	0.2	0.1	0.2
Mg	0.18	0.16	0.32	0.33	0.42	0.29	0.16	0.13	0.1	0.03
Al	1.38	1.6	0.65	2.25	2.73	0.67	1.49	5.6	6.6	1.7
Si	1.66	1.76	2.66	3.92	5.38	4.67	11.12	6.85	22.2	16.1
P	1.32	0.7	0.08	0.23	0.64	0.62	1.1	0.798	2.6	0.6
K	0.04	0.04	0.03	0.27	0.11	0.05	0.09	0.13	0.7	0.4
Ca	0.84	0.69	1.28	1.76	1.87	1.73	1.25	0.61	1.1	0.2
Fe	0.51	0.49	0.22	0.77	0.89	0.24	2.56	0.82	5.6	6.2
O/C	0.4063	0.3494	0.4466	0.4471	0.3183	0.3535	0.0803	0.2004	−1.18	−0.35
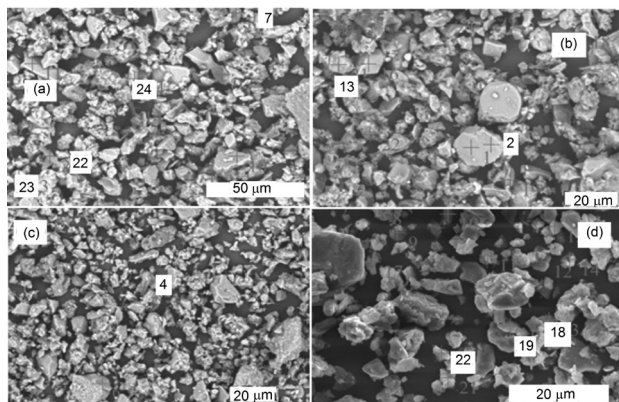
Figure 5. SEM micrographs showing different morphologies of the PyC in the silt fraction (secondary electron images): circular particles (a) and (b): A1/29 sample and other particles from (A2)30 and (A3)31 horizons (c) and (d): (A2)30/ (A3)31 samples.
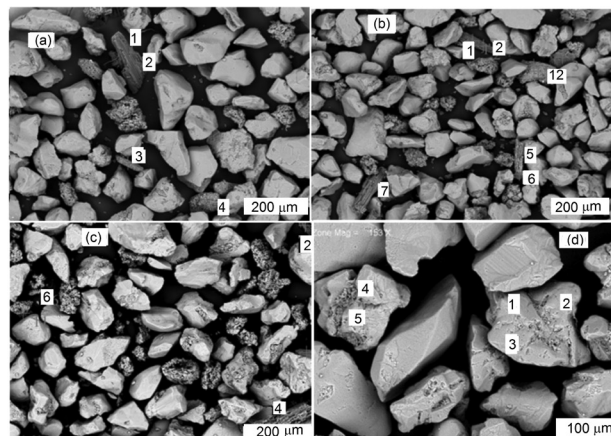

Figure 6. SEM micrographs of sub-samples of the fine sand fraction of the A1, A2 and A3 horizons: (a) and (b): (A1)15; (c): (A2)16 and (d): (A3)17 horizons (backscattering images).

Table 7. EDS results of the selected sub-samples of the silt fractions from the A1, A2, A3 and AB horizons

Element	(A1)29-7 / %	(A1)29-22 / %	(A2) 30-4 / %	(A3) 31-19 / %	(A3)31-22 / %	(AB)32-1 / %	(AB)32-2 / %
C	57.97	64.22	71.31	65.4	63.1	60.54	59.67
O	34.85	29.26	19.59	28.96	28.26	31.49	27.35
Na	0.2	0.16	0.33	0.34	0.38	0.32	0.3
Mg	0.36	0.01	0.1	0.01	0.09	0.03	0.04
Al	0.48	0.1	0.58	0.41	1.8	0.47	2.23
Si	1.86	5.13	6.52	4.46	5.34	5.03	9.28
P	1	0.56	0.74	0.11	0.16	0.13	0.1
K	0.04	0.05	0.12	0.04	0.04	0.05	0.1
Ca	2.76	0.26	0.5	0.14	0.2	0.23	0.2
Fe	0.96	0.22	0.23	0.13	0.62	0.69	0.73
O/C	0.3984	0.2609	0.0388	0.2852	0.2098	0.2912	0.0655

Micromorphological and chemical data of the fine sand fraction

The fine sand fraction of the PyC consisted of particles with elongated shapes from waste charred plants (Figures 6a and 6b). Similar to previous fractions, the fine sand fraction also showed a decreased in the pyrogenic particles toward the lower horizons. At some locations of the analyzed (A1)15, (A2), (A3) and 16/17 sub-samples of the fine sand fraction (Table 8), the Al and Ca concentrations were higher than those observed in the clay and silt fractions.

For the (A3)17 sub-sample, we found that the pyrogenic particles were preferably concentrated in aggregates included within fissures of quartz grains (Figure 6d). This was also observed in a sub-sample of the fine sand fraction of the AB horizon and in the A1 horizon of the coarse sand fraction (AB/AB and 18/43 sub-samples), as well as in other soils types.[34]

Micromorphological and chemical data of the coarse sand fraction

For the (A1)/43 sample, a fraction of coarse sand particles with micromorphological prismatic forms elongated with an irregular surface were identified, which was consistent with pyrogenic particles of the other fractions. Nevertheless, the chemical data resulted in negative results for the O/C ratios values. However, we cannot rule out the occurrence of PyC in this fraction from the ABE profile because of the micromorphological features observed for the (A1)/43 sample. These characteristics were observed in other PyC particles from denser and deeper fractions of soils, which were attributed to alterations

Table 8. EDS results from selected particles from the fine sand fraction of the A1, A2, A3 and AB horizons (15-18 sub-samples, respectively)

Element	15/A1/1 / %	15/A1/2 / %	15/A1/3 / %	16/A2/2 / %	16/A2/4 / %	17/A3/2 / %	17/A3/7 / %	18/AB-1 / %
C	63.1	51.34	50.11	48.27	50.47	46.5	46.47	54.91
O	26.76	31.3	37.83	29.08	31.8	39.74	39.99	35.41
Na	0.05	0.02	0.02	0.15	0.1	0.06	0.056	0.16
Mg	0.4	0.39	0.15	0.9	0.45	0.16	0.29	0.07
Al	0.24	3	0.75	1.06	5.47	3.23	3.59	0.63
Si	2.27	3.65	8.1	2.7	4.13	7.78	6.02	6.27
P	1.47	2.38	0.86	0.97	1.34	0.72	0.76	0.24
K	0.09	0.28	0.07	0.16	0.29	0.12	0.15	0.11
Ca	5.42	5.82	1.63	15.95	4.1	0.83	1.72	0.08
Fe	0.19	1.86	0.5	0.75	1.85	0.85	0.94	2.13
O/C	0.1913	0.0973	0.3188	0.03671	0.1007	0.3322	0.3551	0.3377

suffered by the ABE from charcoal and ceramic particle transportation to deeper horizons.[11]

Distribution of PyC in the horizons fractionated from the ABE profile

PyC particle total of the ABE profile horizons

After monitoring the morphological properties and determining the O/C atomic ratio, the distribution of the particles in the clay, silt, fine sand and coarse sand fractions and in the ABE profile horizons were investigated. The particles of pyrogenic carbon were found to be concentrated preferentially in horizon A1 and A2 (Table 9). The preferential accumulation of PyC in the surface horizons can be attributed to activities undertaken by the ancient inhabitants of the region, with the most common examples being the burning of wood for cooking food, parties and other ceremonies.

Table 9. Total number of PyC particles in clay, silt, fine sand and coarse sand fractions of the ABE profile horizons

Horizon	Clay	Silt	Fine sand	Coarse sand	Total of particles
A1	19	11	26	1	57
A2	23	4	8	0	35
A3	8	7	2	0	17
AB	0	4	1	0	5

By analyzing the distribution of PyC particles along the horizons, the A1 and A2 horizons contributed the most to the high concentrations of PyC in the clay and fine sand fractions. The fact that the fine sand fraction contributed to the increased amount of PyC particles in the horizons is possibly because this fraction showed well-defined

particles that were easy to recognize, thus allowing a better morphological and chemical evaluation.

Classification of the PyC particles according to the O/C ratios from the ABE profile samples

The distinction between the types of particles was made based on the usual method using the O/C ratios obtained from EDS analysis from carbon of various sources,[17,34] such as coal or char, with char having an O/C = 0.4-0.6 and charcoal having an O/C = 0.2-0.4, as well as, condensates of combustion, such as soot with an O/C < 0.2. The firing temperature directly influenced this ratio. The total number of each type of particle was indicated for clay, silt and fine sand from the ABE profile samples (Table 10).

Table 10. Total PyC particles classified as char, charcoal and condensates of combustion in each fraction of the ABE profile horizons

Description	Clay	Silt	Fine sand	Coarse sand
Total char particles	5	1	8	1
Total charcoal particles	25	11	16	0
Total condensates of combustion particles	20	24	13	0

Evaluation of the O/C ratio of CC, charcoal and char from the ABE profile horizons

The PyC types determined according to the O/C ratios and the respective values of average and standard deviation for each fraction in the horizons from the ABE profile are indicated in Table 11. These data are of great importance in the estimation of biomass firing temperatures. It has been found that temperatures above 350 °C and lower than 600 °C are suitable for the production of condensates of combustion, and higher temperature burns produce lower O/C ratios.[8,13,34]

Table 11. Average results obtained for the O/C ratio of the fractionated samples of the ABE profile

Fraction	O/C	SD	n	Type of particles
	0.09	0.07	21	condensed combustion
Clay	0.32	0.05	17	charcoal
	0.43	0.01	8	char
	0.1	0.05	15	condensed combustion
Silt	0.31	0.07	11	charcoal
	0.45	–	1	char
	0.13	0.07	15	condensed combustion
Fine sand	0.34	0.05	14	charcoal
	0.52	0.04	8	char

SD: standard deviation; n: number of measurements on different spots on the particles of pyrogenic carbon.

According to the O/C ratios obtained for the samples fractionated from the ABE profile (Table 11), we suggest that the biomass sources of PyC in this study were equivalent to those considered for the condensates of combustion, such as coniferous wood and charcoal, which are usually produced from the burning of lignin, cellulose and wood. The CC and charcoal types are mainly concentrated in the fine sand, clay and silt fractions in the A1 horizon and in clay in the A2 horizon (Figure 7). The difference in the type of PyC observed is due uneven combustion in an open forest fire.[17]
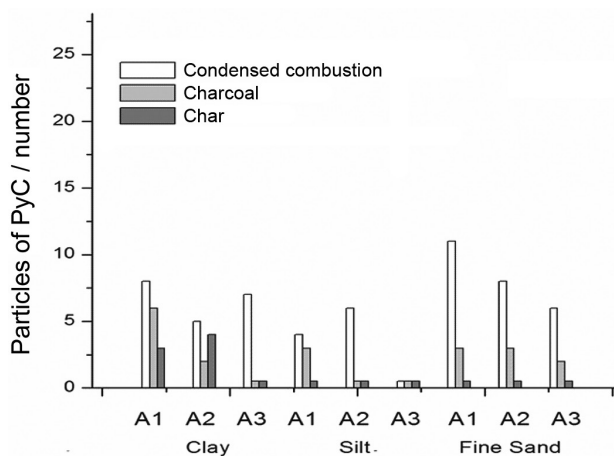
Figure 7. Distribution of pyrogenic carbon in clay, silt and fine sand fractions from the ABE profile horizons.

Conclusions

Micromorphological observations and monitoring of the O/C atomic ratios in fractionated samples of archaeological black earth (ABE) profiles from the Ilha de Terra site in the Caxiuanã Region showed the presence of pyrogenic carbon (PyC) particles with the following characteristics:

A significant decrease was found in the possible forms of PyC from horizons of the ABE profile, which occur in the following order: A1 > A2 > A3 > AB.

The particles of pyrogenic carbon were identified according to the mean values of the O/C ratios from the clay, silt and fine sand fractions and were classified as condensed combustion (0.09, 0.1 and 0.13), charcoal (0.32, 0.31 and 0.34) and char (0.43, 0.45 and 0.52), respectively.

Pyrogenic carbon was accumulated preferentially in the A1 and A2 horizons due to the burning of wood for the cooking of food, parties and other activities performed by the ancient inhabitants of the Ilha de Terra of the Caxiuanã Region.

The amounts of the PyC particles types follow the order: condensed combustion > charcoal > char and the highest concentrations of condensed combustion were found to occur in the clay fraction.

The O/C ratios obtained in this study indicate that the firing temperatures of the biomass source of the PyC particles are closer to 600 °C (rather than 350 °C). This temperature is consistent with evidence of anthropogenic activities from the Ilha de Terra site.

The types of particles identified in the Ilha de Terra site suggest that the biomass sources of pyrogenic carbon could be wood, cellulose or lignin.

Acknowledgments

References

1. Preston, C. M.; Schmidt, M. W. I.; *Biogeosciences* **2006**, *3*, 397.

2. Wolf, M.; Lehndorff, E.; Wiesenberg, G. L. B.; Stockhausen, M.; Schwark, L.; Amelung, W.; *Org. Geochem.* **2013**, *55*, 21.

3. Jorio, A.; Ribeiro-Soares, J.; Cançado, L. G.; Falcão, N. P. S.; Santos, H. F.; Baptista, D. L.; Ferreira, E. H. M.; Archanjo, B. S.; Achete, C. A.; *Soil Tillage Res.* **2012**, *122*, 61.

4. González-Pérez, J. A.; González-Vila, F. J.; Almendros, G.; Knicker, H.; *Environ. Int.* **2004**, *30*, 855.

5. Glaser, B.; Amelung, W.; *Global Biogeochem. Cycles* **2003**, *17*, 33.

6. Glaser, B.; Birk, J. J.; *Geochim. Cosmochim. Acta* **2012**, *82*, 39.

7. Kuhlbusch, T. A. J.; Andreae, M. O.; Cachier, H.; Goldammer, J. G.; Lacaux, P.; Shea, R.; Crutzen, P. J. J.; *Geophys. Res.* **1996**, *101*, 651.

8. Simpson, M. J.; Hatcher, P. G.; *Org. Geochem.* **2004**, *35*, 923.

9. Scott, A. C.; Damblon, F.; *Paleogeogr., Paleoclim., Paleoecol.* **2010**, *291*, 10.

10. Glaser, B.; Haumaier, L.; Guggenberger, G.; Zech, W.; *Org. Geochem.* **1998**, *29*, 811.

11. Glaser, B.; Balashov, E.; Haumaier, L.; Guggenberger, G.; Zech, W.; *Org. Geochem.* **2000**, *31*, 669.

12. Glaser, B.; Haumaier, L.; Guggenberger, G.; Zech, W.; *Naturwissenschafter* **2001**, *88*, 37.

13. Schmidt, E. M.; Skjemstad, J. O.; Glaser, B.; Knicker, H.; Kögel-Knabner, I.; *Geoderma* **2002**, *107*, 71.

14. Czimczik, C. I.; Preston, C. M.; Schmidt, M. W. I.; Werner, R. A.; Schulze, E. D.; *Org. Geochem.* **2002**, *33*, 1207.

15. Hammes, K.; Smernik, R. J.; Skjemstad, J. O.; Schmidt, M. W. I.; *Appl. Geochem.* **2008**, *23*, 2113.

16. Fu, F.; Jiang, M.; Wu, Y.; Lin, G.; Xu, L.; Chen, Z.; *Sci. Total Environ.* **2011**, *409*, 4449.

17. Stoffyn-Egli, P.; Potter, T. M.; Leonard, J. D.; Pocklington, R.; *Sci. Total Environ.* **1997**, *198*, 211.

18. Brodowski, S.; Amelung, W.; Haumaier, L.; Zech, W.; *Geoderma* **2007**, *139*, 220.

19. de La Rosa, J. M.; García, L. S.; de Andrés, J. R.; González-Vila, F. J.; González–Pérez, J. A.; Knicker, H.; *Quaternary Int.* **2011**, *243*, 264.

20. Kuzyakov, Y.; Bogomolova, I.; Glaser, B.; *Soil Biol. Biochem.* **2014**, *70*, 229.

21. Chia, C.; Munroe, P.; Joseph, S.; Lin, Y.; Lehmann, J.; Muller, D.; Xin, H.; Neves, E.; *J. Microsc.* **2011**, *245*, 129.

22. Novotny, E. H.; Hayes, M. H. B.; Azevedo, E. R.; Bonagamba, T. J.; *Naturwissenschaften* **2006**, *93*, 447.

23. Smith, N. J. H.; *Ann. Assoc. Am. Geogr.* **1980**, *70*, 553.

24. Lima, H.; Schaefer, C.; Mello, J.; Gilker, R.; Ker, J.; *Geoderma* **2002,** *110*, 1.

25. Solomon, D.; Lehmann, J.; Thies, J.; Schäfer, T.; Liang, B.; Kinyangi, J.; Neves, E.; Petersen, J.; Luizão, F.; Skjemstad, J.; *Geochim. Cosmochim. Acta* **2007**, *71*, 2285.

26. Neves, E. G.; Petersen, J. B.; Bartone, R. N.; Silva, C. A. In *Historical and Socio-Cultural Origins of Amazonian Dark Earths*; Lehmann, J.; Kern, D. C.; Glaser, B.; Woods, W. I., eds.; Kluwer Academic Publishers: Dordrecht, 2003, ch. 3.

27. Kern, D. C.; Aquino, G.; Rodrigues, T.; Frazão, F.; Sombroek, W.; Myers, T.; Neves, E. In *Amazonian Dark Earths: Origin, Properties, Management*; Lehmann, J., Kern, D., Glaser, B., Woods, W., eds.; Kluwer Academic Publishers: Boston-London, 2003, ch. 4.

28. Kern, D. C.; Kampf, N.; Woods, W.; Denevan, W.; Costa, M. L.; Frazão, F.; Sombroek, W. In *As Terras Pretas de Índio da Amazônia: sua Caracterização e uso deste Conhecimento na Criação de Novas Áreas*; Teixeira, W.; Kern, D. C.; Madari, B.; Lima, H.; Woods, W., eds.; Associação Brasileira das Editoras Universitárias: São Paulo, 2010.

29. Costa, M. L.; Kern, D. C.; *J. Geochem. Expl.* **1999**, *66*, 369.

30. Wells, E.; Terry, R.; Parnell, J.; Hardin, P.; Jackson, M.; Houston, S.; *J. Archaeol. Sci.* **2000**, *27*, 449.

31. Costa, M. L.; Rios, G. M.; Silva, M. C.; Silva, G. J.; Molano-Valde, U.; *Rev. Esc. Minas* **2011,** *64*, 17.

32. Costa, J. A.; Costa, M. L.; Kern, D. C.; *J. Archaeol. Sci.* **2013**, *40*, 2771.

33. Brodowski, S.; Amelung, W.; Haumaier, L.; Zech, W.; *Geoderma* **2007**, *139,* 220.

34. Brodowski, S.; Amelung, W.; Haumaier, L.; Abetz, C.; Zech, W.; *Geoderma* **2005**, *128*, 116.

35. Fernandes, M. B.; Skjemstad, J. O.; Johnson, B. B.; Wells, J. D.; Brooks, P.; *Chemosphere* **2003**, *51*, 785.

36. Rose, N. L.; Juggins, S.; Watt, J.; Battarbee, R.W.; *Ambio* **1994,** *23*, 296.

37. Kern, D. C.; Costa, J. A.; Aquino, G.; Kampf, N.; Costa, F. A.; Costa, M. L.; Ruivo, M. L. P.; Lemos, V. P.; Frazão, F. J. In *Caxiuanã: Paraíso Ainda Preservado*; Silva, J.; Botelho, A.; Pinheiro, A., eds.; Associação Brasileira das Editoras Universitárias: São Paulo, 2013, p. 165.

38. Lisboa, P. L. B.; *Estação Científica Ferreira Pena/ECFPn-Caxiuanã*; Museu Paraense Emílio Goeldi: Belém, 1997.

39. Rocha, S. F. R.; Ferreira, M. R. C.; Sablayrolles, M. G. P. In *Caxiuanã: Paraíso Ainda Preservado*; Silva, J.; Botelho, A.; Pinheiro, A., eds.; Associação Brasileira das Editoras Universitárias: São Paulo, 2013, p. 257.

40. Departamento Nacional de Produção Mineral; *Projeto RADAM Brasil*: Rio de Janeiro, 1974.

41. Munsell Color Company X-Rite; *Munsell Soil Colors Charts*; 1994 revised edition; Munsell Color Company, X-Rite: Baltimore, 2000, p. 50.

42. Lemos, A.; Santos, P. B.; *Manual de Descrição e Coleta de Solos em Campo*; Sociedade Brasileira de Ciência do Solo: Viçosa, 2002.

43. Lemos, V. P.; Costa, M. L.; Gurjão, R. S.; Kern, D. C.; Mescouto, C. S. T.; Lima, W. T. S.; Valentim, T. L.; *Rev. Esc. Minas* **2009**, *62,* 139.

44. Gurjão, R. S.; Lemos, V. P.; Costa, M. L.; Dantas Filho, H. A.; Dantas, K. G. F.; Lima, W. T. S.; *Quim. Nova* **2010**, *33*, 821.

45. Efron, B.; *J. Am. Stat. Assoc.* **2004**, *99*, 619.